



Nonlinear Optical Rectification, the Second and Third Harmonic Generation in Asymmetric Double Quantum Well Under the Intense Laser Field

Ünal YESILGUL^a, Emre Bahadır AL^b, Fatih UNGAN^{a,*}, Esin KASAPOGLU^b

^a*Faculty of Technology, Department of Optical Engineering, Cumhuriyet University, 58140 Sivas, Turkey*

^b*Faculty of Science, Physics Department, Cumhuriyet University, 58140 Sivas, Turkey*

Received: 04.11.2016; Accepted: 14.11.2016

Abstract. In this study, the effects of a non-resonant intense laser field and the Al-concentration on the optical rectification, second and third harmonic generation in asymmetric double quantum well are investigated within the compact density matrix approach theoretically. The results show that the intense laser field and the Al-concentration lead to significant changes in the coefficients of nonlinear optical rectification, second and third harmonic generations.

Keywords: Asymmetric double quantum well, Nonlinear optical rectification, Second and third harmonic generations, Intense laser field

Yoğun Lazer Alanı Altındaki Asimetrik Çift Kuantum Kuyusunun Doğrusal Olmayan Optik Düzeltme, İkinci ve Üçüncü Harmonikleri

Özet. Bu çalışmada, asimetrik çift kuantum kuyusunun doğrusal olmayan optik düzeltme, ikinci ve üçüncü harmonikleri üzerine Al-konsantrasyonu ve rezonans olmayan yoğun lazer alanının etkisi kompakt yoğunluk matris yaklaşımı kullanılarak teorik olarak incelenmiştir. Sonuçlar, yoğun lazer alanı ve Al-konsantrasyonun doğrusal olmayan optik düzeltme, ikinci ve üçüncü harmonikler üzerine önemli değişmelere neden olduğunu göstermektedir.

Anahtar Kelimeler: Asimetrik çift kuantum kuyusu, doğrusal olmayan optik düzeltme, ikinci ve üçüncü harmonik üretimler, yoğun lazer alanı

1. INTRODUCTION

Optical properties of semiconductor nanostructures have received considerable attention over the last 15 years [1–9]. In this area, it was interested in semiconductor quantum well (QW) structures which are characterized by an asymmetric double confining potential due to their potential applications in electronic and optical devices [10–13]. The asymmetry of confining potential can be generated by either advanced material growing technology, such as molecular-beam epitaxy and metallicorganic chemical vapor deposition, or by the implementation of a static electric field to a nanostructure with symmetric confining potential.

Among the nonlinear optical processes in semiconductor nanostructures, attention has turned to the second-order nonlinear optical properties, such as nonlinear optical rectification (NOR) [14–17] and second-harmonic generation (SHG) [18–20] and third-order nonlinear optical properties, such as third-harmonic generation (THG) [21–24]. If a quantum system show significant asymmetry, second-order nonlinear processes usually have strong magnitude than the high-order nonlinear processes.

* Corresponding author. *Email address:* fungan@cumhuriyet.edu.tr

Accordingly, impurities such as confined donors and acceptors in the QWs have been studied intensively [25–28]. Several numerical methods have been developed to systematically investigate the physical properties of impurities embedded in a QW. In many current areas of the chemistry and physics, an asymmetric double quantum wells (ADQW) potential has some distinctive properties contrast to the relatively simple case of the symmetrical double QW potential.

As known, the second order nonlinear susceptibility in a symmetric QW structure is negligible except for a small contribution from bulk susceptibility. But when the symmetry broken, non-zero contributions to the second-order nonlinear optical susceptibility are expected to appear. For example, a detailed investigation of the second harmonic generation in symmetrical and asymmetrical Gaussian potential QWs under the influence of applied electric field by using the compact-density-matrix approach and the finite difference method is given by Yuan et al. [18] and their results show that the magnitude of SHG which depend dramatically on the applied electric field and the structural parameters susceptibility can reach a large order. Electric-field-induced SHG in the asymmetrical Gaussian potential QWs is investigated by Zhai [19] using the effective mass approximation employing the compact density matrix method and the iterative approach. Mou et al. [20] show that both σ and U_0 , which are parameters of the asymmetrical semi-exponential QW, have great influences on the magnitude and the resonant frequency of SHG coefficients.

While the second-order susceptibility disappears due to the inversion symmetry, the third-order susceptibility has a very large increase compared with the bulk material. Therefore, for low-dimensional quantum systems without inversion symmetry, often without taking into account the third-order nonlinear optical properties, focused on only the second-order nonlinear optical properties. But, in low dimensional systems with inversion symmetry, third-order nonlinear optical properties can be taken into account. For this purpose, the THG coefficients in a QW with hydrogenic impurity are theoretically investigated by Zhang et al. [21] with the compact-density-matrix approach and iterative method and they show that the THG coefficients are strongly affected by the hydrogenic impurity. Zhai et al. [22] show that the absolute value, the imaginary and real parts of the THG coefficients are greatly influenced by the parabolic confinement frequency and the characteristic parameter of the inverse squared potential. Niculescu et al. [23] found that an axial orientation of the field allows the third harmonic generation and that process is enhanced for a particular polarization of the incident light and a proper field strength. Mou et al. [24] show that both the amount of peaks of THG coefficients and the magnitude of peaks are significantly affected by σ and U_0 .

In this study, we have investigated the effects of the ILF and Al-concentration on NOR, SHG and THG in an ADQW by using the compact density matrix approach. This article is organized as follows: In Section 2, the details of the calculations are presented. In Section 3, numerical results are presented and discussed. Finally, Section 4 contains the main results of this paper.

2. THEORY

In this study, we have investigated the effects of ILF and Al-concentration on electronic states in a GaAs/Ga_{1-x}Al_xAs ADQW grown along the z -direction. The schematic representation of the ADQW for different ILF parameters is given in the Fig. 1 (a-c). The method used in the present calculation is based on a non-perturbative theory developed to describe the atomic behavior in high-frequency ILFs [29–31]. Within the framework of effective mass approach, the Hamiltonian for an electron in the ADQW in the presence of ILF with linear polarization parallel to the growth direction is given by

$$H = \frac{1}{2 m_e^*} (\vec{p}_e)^2 + V(z, \alpha_0), \quad (1)$$

where m_e^* is the electron effective mass, \vec{p}_e is the electron momentum operator, z represents the growth direction, $\alpha_0 = \frac{eF_0}{m_e^* \omega^2}$ is the laser dressing parameter, F_0 is the field strength, ω is the non-resonant frequency of the laser field, and $V(\alpha_0, z)$ is the 'dressed' confinement potential which is given by the following expression:

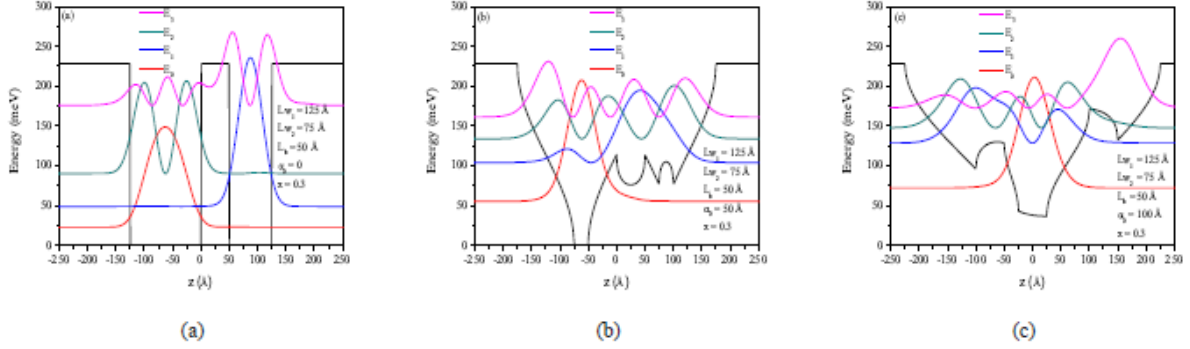


Fig. 1 Potential profiles, the wave functions and related energy levels for three different α_0 values: (a) $\alpha_0 = 0$, (b) $\alpha_0 = 50 \text{ \AA}$ and (c) $\alpha_0 = 100 \text{ \AA}$.

$$\begin{aligned} V(z, \alpha_0) = & V_0 \Theta(-\alpha_0 - z - L/2) + \frac{V_0}{\pi} \arccos\left(\frac{L/2 + z}{\alpha_0}\right) [1 - \Theta(-\alpha_0 - L/2 - z)] \Theta(\alpha_0 - L/2 - z) \\ & + V_0 \Theta(-\alpha_0 + z - L/2) + \frac{V_0}{\pi} \arccos\left(\frac{L/2 - z}{\alpha_0}\right) [1 - \Theta(-\alpha_0 - L/2 + z)] \Theta(\alpha_0 - L/2 + z) \\ & + V_0 [1 - \Theta(-\alpha_0 - z)] - \Theta(-\alpha_0 + z)] \\ & + \frac{V_0}{\pi} \left[\arccos\left(\frac{z}{\alpha_0}\right) [1 - \Theta(-\alpha_0 - z)] \Theta(\alpha_0 - z) + \arccos\left(\frac{-z}{\alpha_0}\right) [1 - \Theta(-\alpha_0 + z)] \Theta(\alpha_0 + z) \right] \\ & + V_0 [1 - \Theta(-\alpha_0 - z)] - \Theta(-\alpha_0 - L_B + z)] \\ & - \frac{V_0}{\pi} \left[\arccos\left(\frac{z}{\alpha_0}\right) [1 - \Theta(-\alpha_0 - z)] \Theta(\alpha_0 - z) + \arccos\left(\frac{L_B - z}{\alpha_0}\right) [1 - \Theta(-\alpha_0 - L_B + z)] \Theta(\alpha_0 - L_B + z) \right], \end{aligned} \quad (2)$$

where Θ is the Heaviside unit step function, $L = L_L + L_B + L_R$ is the effective width of ADQW structure, L_B is the central barrier width and L_L (L_R) is the left (right) well.

After the energies and related wave functions for the Hamiltonian in Eq.(1) are obtained, by using the compact density matrix method and an iterative procedure, the expressions of NOR, SHG and THG for the ADQW system can be obtained. NOR, SHG and THG susceptibilities can be expressed respectively as follows [32, 33]:

$$\chi_0^{(2)} = \frac{4e^3 \rho_v}{\epsilon_0 \hbar^2} \mu_{10}^2 \delta_{10} \frac{E_{10}^2 (1 + \Gamma_2/\Gamma_1) + \hbar^2 (\omega^2 + \Gamma_2^2) (\Gamma_2/\Gamma_1 - 1)}{[(E_{10} - \hbar\omega)^2 + \hbar^2 \Gamma_2^2] [(E_{10} + \hbar\omega)^2 + \hbar^2 \Gamma_2^2]}, \quad (3)$$

$$\chi_{2\omega}^{(2)} = \frac{e^3 \rho_v}{\epsilon_0} \frac{\mu_{10} \mu_{21} \mu_{20}}{(\hbar\omega - E_{10} - i\hbar\Gamma_3)(2\hbar\omega - E_{20} - i\hbar\Gamma_3)}, \quad (4)$$

$$\chi_{3\omega}^{(3)} = \frac{e^4 \rho_v}{\epsilon_0} \frac{\mu_{10} \mu_{21} \mu_{32} \mu_{30}}{(\hbar\omega - E_{10} - i\hbar\Gamma_3)(2\hbar\omega - E_{20} - i\hbar\Gamma_3)(3\hbar\omega - E_{30} - i\hbar\Gamma_3)}. \quad (5)$$

where e is the electron charge, ρ_v is the electronic density, ϵ_0 is the permittivity of the free space, \hbar is the reduced Planck constant, $\mu_{ij} = \langle \psi_i | z | \phi_j \rangle$ ($i, j = 0, 1, 2, 3$) is the dipole matrix element, $\delta_{10} = |\mu_{00} - \mu_{11}|$, $E_{ij} = E_i - E_j$ is the transition energy, $\Gamma_k = 1/T_k$ (where $k = 1, 2, 3$) is damping term about the lifetime of the electrons involved in the transitions and ω is the frequency of the incident photons.

3. RESULTS AND DISCUSSION

In this study, we examined the effects of ILF and Al-concentration on NOR, SHG and THG in the GaAs/Ga_{1-x}Al_xAs ADQW. Values of the physical parameters used in the calculations are: $L_L = 125 \text{ \AA}$,

$L_B = 50 \text{ \AA}$, $L_R = 75 \text{ \AA}$, $m_e^* = 0.063m_0$ (where m_0 is the free electron mass), $\rho_v = 1.0 \times 10^{23} \text{ m}^{-3}$, $T_1 = 1 \text{ ps}$, $T_2 = 0.2 \text{ ps}$, and $T_3 = 0.5 \text{ ps}$.

In the Figs. 2 (a) and (b), we present the energy differences as a function of the ILF and Al-concentration, respectively. Increment or decrement in the energy differences (or energy levels taken into consideration) reflects the geometrical confinement due to the variation of the effective well width (L) with the effect of ILF: as α_0 increases, bottom width of the well decreases while the top width increases. The variation of energy differences versus ILF provide the necessary information for the physical description of the characteristics of NOR, SHG and THG. As Al concentration increases, the potential barrier and accordingly energy levels increase. However, the increase in the upper energy levels is more than the increase in the level of the ground state energy.

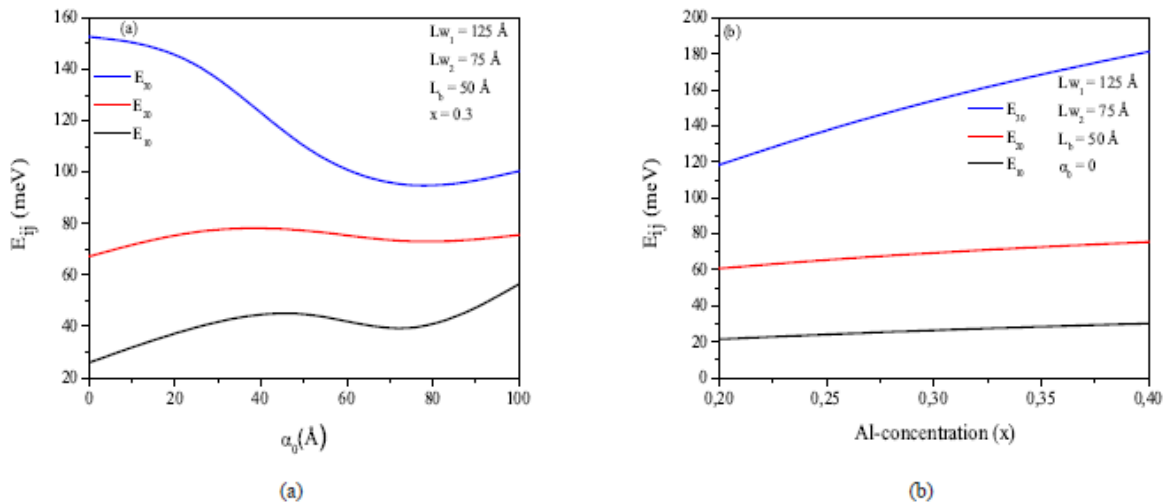


Fig. 2 The energy differences as a function of (a) the ILF parameter and (b) Al-concentration.

In the Figs. 3, we show the NOR as a function of photon energy for different values of the ILF parameter and Al-concentration. As ILF parameter increases, we can see in Fig. 3(a) that NOR shows a blue-shift. The reason for this is the change of μ_{10} , δ_{10} and E_{10} values as ILF parameter increases. At the same time, the peak value of NOR firstly increases and then decreases as ILF parameter increases and the maximum peak is seen at $\alpha_0 = 50 \text{ \AA}$. In Fig. 3(b), NOR has been reported as a function of the incident photon energy for different values of Al-concentration. As the Al-concentration increases, NOR clearly shifts to the high energies (blue-shift). The main causes of this blue shift are the change of the parameters μ_{10} , δ_{10} and E_{10} . However, as the Al-concentration increases, the peak value becomes lower.

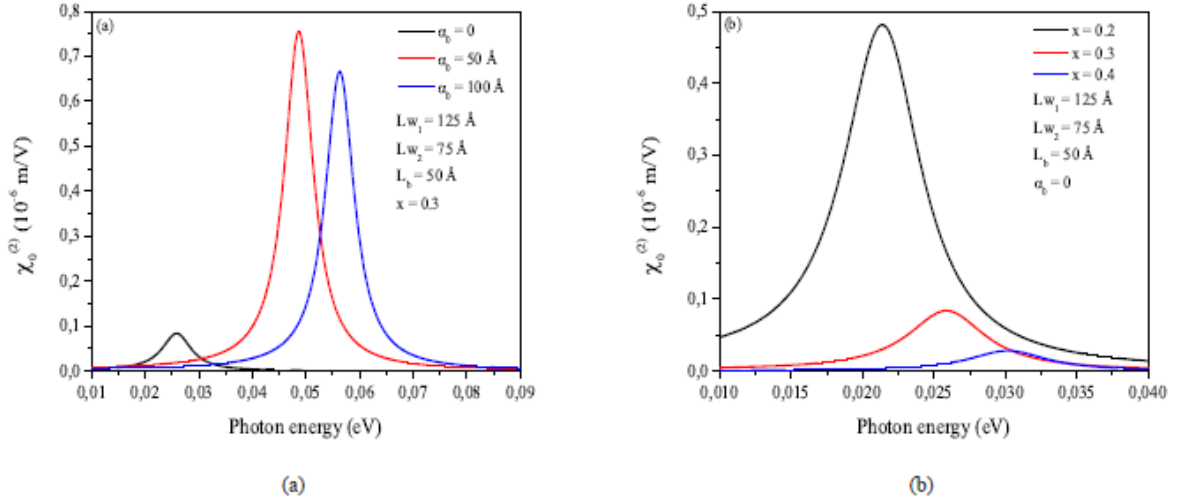


Fig. 3 The variations of the NOR as a function of photon energy for different values of (a) the ILF parameter and (b) Al-concentration.

The spectrum of the SHG for different values of the ILF parameter and the Al-concentration is given in the Figs. 4 (a) and (b), respectively. Fig. 4(a) shows that SHG is shown graphically corresponding to photon energy for three different values of the ILF parameter. This figure shows that SHG has two peaks which are located in the vicinity of $\hbar\omega = E_{10}$ and $\hbar\omega = E_{20}/2$ for each value of the ILF taken into consideration. As ILF parameter increases, the resonance peak of SHG firstly shifts to the higher energies (blue-shift) and then shifts to the lower energies (red-shift). In addition, the magnitude of the resonance peak of SHG also firstly increases and then decreases depending on the ILF parameter. The cause of the above results is as follows: As ILF increases, firstly, the narrow well (Lw_2) becomes shallow, larger well becomes narrow and extending of the ground state wave function decreases while extending of wave functions in the upper states increase. Therefore, the magnitude of the resonance peak of SHG firstly increases and then geometric confinement becomes weak, extending of the all wave functions increase, thus the magnitude of the resonance peak of SHG is reduced. Fig. 4(b) shows the SHG coefficient versus the incident photon energy for different values of the Al-concentration. As the Al-concentration increases, resonance peaks of SHG shift to the blue with decreasing the magnitude.

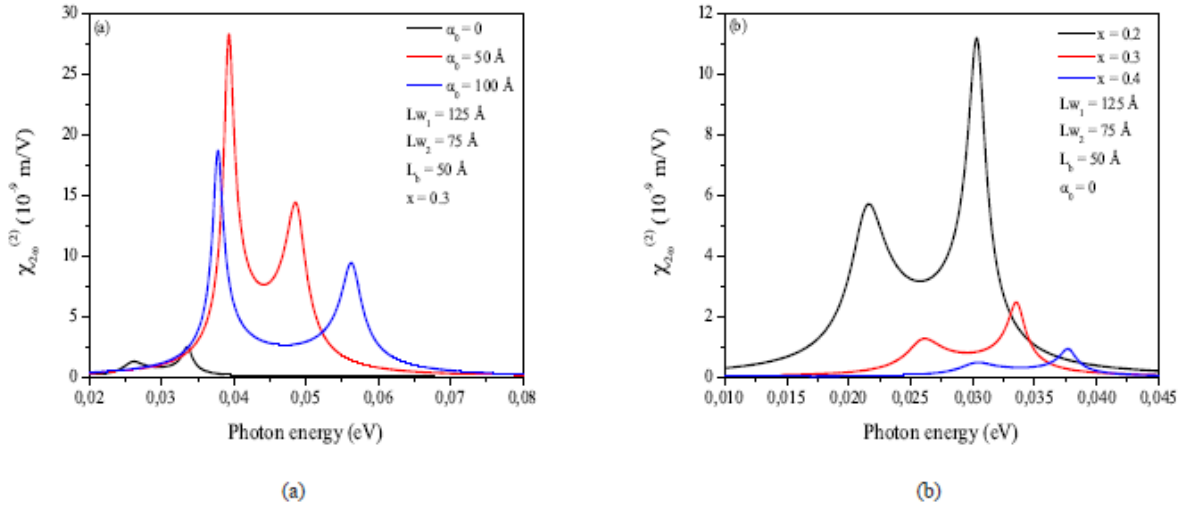


Fig. 4 The variations of the SHG as a function of photon energy for different values of (a) the ILF parameter and (b) Al-concentration.

Figs. 5 (a) and (b) show the variation of the THG coefficients as a function of the incident photon energy for different α_0 values and the Al-concentrations, respectively. From these figures, it can be seen that: (i) As α_0 increases, the magnitude of the resonance peak firstly increases and then decreases which is related to the dipole moment matrix elements μ_{10} , μ_{21} , μ_{32} and μ_{30} and the peak of THG coefficient firstly shifts to the blue and then shifts to the red. (ii) Increment in the Al-concentration creates amendments in the THG coefficient; especially for $x = 0.3$ the magnitude of the THG increases more than that of NOR and SHG (it should be noted that; the curves for $x = 0.3$ and $x = 0.4$ are multiplied by 10^{-1} and 10^2 , respectively), and the peak position of the THG shifts to the blue with increasing Al-concentration.

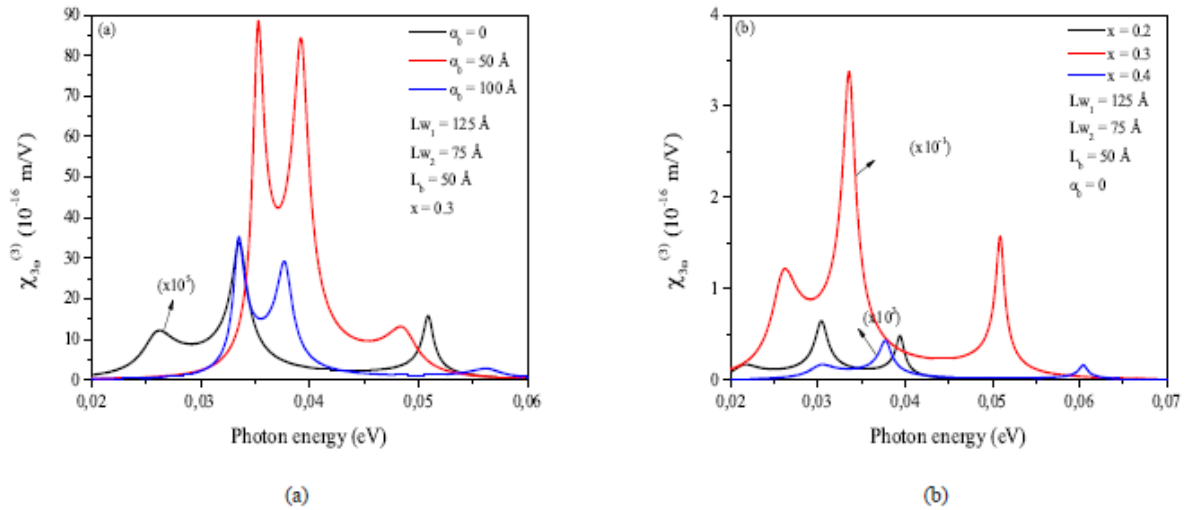


Fig. 5 The variations of the THG as a function of photon energy for different values of (a) the ILF parameter and (b) Al-concentration.

4. CONCLUSIONS

As a result, based on the density matrix approach, NOR, SHG and THG coefficients of the GaAs/Ga_{1-x}Al_xAs ADQW were analyzed theoretically for different Al-concentrations and non-resonant ILF values. Our results show that it is possible to identify either red or blue shifts in the resonant peak positions of the NOR, SHG and THG coefficients resulting from the variation of ILF intensity and the Al concentration. As a result, we can tune the electronic structure and main optical properties of the

system depend on intersubband transitions by changing the Al concentration together with the non-resonant intense laser field.

5. ACKNOWLEDGEMENTS

The authors are grateful to The Scientific Research Project Fund of Cumhuriyet University under the project number F-470, TEKNO-007.

REFERENCES

1. P. Horley, Y. V. Vorobiev, V. P. Makhniy, V. M. Sklyarchuk, *Physica E* 83 (2016) 227.
2. D. J. V. Raj, C. J. Raj, S. J. Das, *Superlatt. Microstruct.* 85 (2015) 274.
3. J. Buha, *Appl. Surf. Sci.* 321 (2014) 457.
4. H. Saghrouni, A. Missaoui, R. Hannachi, L. Beji, *Superlatt. Microstruct.* 64 (2013) 507.
5. B. Sonawane, V. Shelke, M. Bhole, D. Patil, *J. Phys. Chem. Solids* 72 (2011) 1442.
6. Moholkar, G. Agawane, K.-U. Sim, Y. bin Kwon, K. Rajpure, J. Kim, *Appl. Surf. Sci.* 257 (2010) 93.
7. G. Sinha, S. Chaudhuri, *Mater. Chem. Phys.* 114 (2009) 644.
8. O. Govorov, *C. R. Phys.* 9 (2008) 857.
9. V. Capozzi, G. Perna, P. Carmone, A. Gallone, M. Lastella, E. Mezzenga, G. Quartucci, M. Ambrico, V. Augelli, P. Biagi, T. Ligonzo, A. Minafra, L. Schiavulli, M. Pallara, R. Cicero, *Thin Solid Films* 511 (2006) 362.
10. U. Yesilgul, E. Al, J. Martinez-Orozco, R. Restrepo, M. Mora-Ramos, C. Duque, F. Urgan, E. Kasapoglu, *Opt. Mater.* 58 (2016) 107.
11. U. Yesilgul, F. Urgan, E. Kasapoglu, H. Sari, I. Sökmen, *Physica B* 475 (2015) 110.
12. E. Al, F. Urgan, U. Yesilgul, E. Kasapoglu, H. Sari, I. Sökmen, *Opt. Mater.* 47 (2015) 1.
13. N. Zeiri, N. Sfina, S. A.-B. Nasrallah, M. Said, *Optik* 39 (2003) 377.
14. X. Liu, L. Zou, C. Liu, Z. Zhang, J. Yuan, *Opt. Mater.* 53 (2016) 218.
15. Z. Zhang, L. Zou, K. Guo, J. Yuan, *Opt. Commun.* 359 (2016) 316.
16. S. Shojaei, A. S. Vala, *Physica E* 70 (2015) 108.
17. F. Urgan, J. Martinez-Orozco, R. Restrepo, M. Mora-Ramos, E. Kasapoglu, C. Duque, *Superlatt. Microstruct.* 81 (2015) 26.
18. J. Yuan, N. Chen, H. Mo, Y. Zhang, Z. Zhang, *Superlatt. Microstruct.* 88 (2015) 389.
19. W. Zhai, *Physica B* 454 (2014) 50.
20. S. Mou, K. Guo, G. Liu, B. Xiao, *Physica B* 434 (2014) 84.
21. Z. Zhang, K. Guo, S. Mou, B. Xiao, L. Liao, *Superlatt. Microstruct.* 76 (2014) 1.
22. W. Zhai, H. Hassanbadi, L. Lu, G. Liu, *Int. J. Nonlin. Mech.* 82 (2016) 69.
23. E. Niculescu, M. Cristea, A. Radu, *Physica E* 57 (2014) 138.
24. B. X. S. Mou, Kangxian Guo, *Superlatt. Microstruct.* 65 (2014) 309.
25. H. Akbas, S. Sucu, S. Minez, C. Dane, O. Akankan, I. Erdogan, *Superlatt. Microstruct.* 94 (2016) 131.
26. P. Baser, I. Altuntas, S. Elagoz, *Superlatt. Microstruct.* 92 (2016) 210.
27. T. Pereira, A. Sousa, M. Degani, G. Farias, *Physica E* 66 (2015) 81.
28. C. Xia, H. Zhang, J. An, S. Wei, Y. Jia, *Physica E* 58 (2014) 43.
29. S. Sakiroglu, U. Yesilgul, F. Urgan, C. A. Duque, E. Kasapoglu, H. Sari, I. Sökmen, *J. Lumin.* 132 (2012) 1584.
30. F. Urgan, U. Yesilgul, S. Sakiroglu, E. Kasapoglu, H. Sari, I. Sökmen, *Phys. Lett. A* 374 (2010) 2980.
31. N. Eseau, *Phys. Lett. A* 374 (2010) 1278.
32. S. Sakiroglu, F. Urgan, U. Yesilgul, M. Mora-Ramos, C. Duque, E. Kasapoglu, H. Sari, I. Sökmen, *Phys. Lett. A* 376 (2012) 1875.
33. C. D. J.C. Martinez-Orozco, M.E. Mora-Ramos, *J. Lumin.* 132 (2012) 449.